2016 International Symposium on Nonlinear Theory and Its Applications,
NOLTA2016, Yugawara, Japan, November 27th-30th, 2016

Reproduction of nonlinear cochlea response by asynchronous bifurcation processor

Kentaro Takeda† and Hiroyuki Torikai

†Department of Computer Science, Kyoto Sangyo University
1–3 Motoyama, Kamigamo, Kitaku, Kyoto 605-8555, Japan
Email: g1344793@cse.kyoto-su.ac.jp, torikai@cse.kyoto-su.ac.jp

Abstract—Biological cochleae have highly nonlinear responses to sound stimuli, e.g., response curves (so-called tuning curves) are highly nonlinear with respect to stimulation frequencies. In this paper, the nonlinear dynamics of a Hopf-bifurcation-type cochlea model based on a concept of an asynchronous bifurcation processor is investigated. It is shown that the model can reproduce nonlinear tuning curves of not only a mammalian cochlea (cat) but also a reptilian cochlea (turtle).

1. Introduction

Biological cochleae have highly nonlinear responses to sound stimuli such as nonlinear frequency tuning curve, multi-tone suppression, first and second pitch shifts, adaptation, parallel spike density encoding, and so on [1]. Among such nonlinear responses, the nonlinear frequency tuning curve is focused in this paper. Fig. 1 shows an example of the frequency tuning curve of a reptilian cochlea (turtle). In this figure, a frequency at a minimum peak of the curve is called a characteristics frequency and is corresponding to a specific position of a basilar membrane in the cochlea, i.e., the basilar membrane works as a kind of nonlinear mechanical Fourier transformer. There are many mathematical and circuit models the cochlea [2]-[10]. One of simple-but-powerful mathematical cochlea models is the Hopf-cochlea [6]-[10]. On the other hand, our group has been developing a neural system modeling approach based on the nonlinear dynamics of an asynchronous cellular automaton, where nonlinear dynamics (especially, bifurcations) of neural systems are reproduced by the asynchronous cellular automaton with low hardware cost [10]-[12]. Our group is conceptually referring to such a hardware platform as "asynchronous bifurcation processor (ABP)."

In this paper, a cochlea model based on the ABP and the Hopf-cochlea is investigated. It is newly shown that the model can reproduce nonlinear tuning curves of an reptilian cochlea (turtle). Note that our previous work suggests the model can reproduce a mammalian cochlea (cat) [10], and thus this paper suggests that the model can be used to model cochleae of many species.

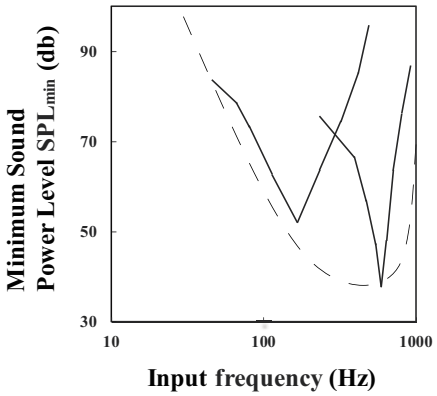

Figure 1: Rough sketch of frequency tuning curves of a reptilian (turtle) cochlea [13].

2. Cochlea Model based on Asynchronous Bifurcation Processor

Let

$$t \in \boldsymbol{R}$$

be a continuous time and let

$$x_1 \in \boldsymbol{R}, \quad x_2 \in \boldsymbol{R}$$

be continuous states. Also, let $\alpha \in \boldsymbol{R}$ be a continuous parameter. Then the following set of equations are known as the normal form of the Hopf-bifurcation [14].

$$\frac{dx_1}{dt} = \alpha x_1 - x_2 + x_1(x_1^2 + x_2^2),$$
$$\frac{dx_2}{dt} = x_1 + \alpha x_2 + x_2(x_1^2 + x_2^2).$$

Based on the normal form of the Hopf-bifurcation, cochlea models have been presented and investigated [8]-[10].

On the other hand, in this paper, the following four discrete states $\{X, Y, P, Q\}$ are used in a cochlea model.

$$X \in \boldsymbol{Z}_N = \{0, \cdots, N-1\}, \qquad Y \in \boldsymbol{Z}_N,$$
$$P \in \boldsymbol{Z}_M = \{0, \cdots, M-1\}, \qquad Q \in \boldsymbol{Z}_M,$$

where N and M are positive integers, which determine the resolution of the state space $\{(X, Y, P, Q) \mid X \in \boldsymbol{Z}_N, Y \in$

$\boldsymbol{Z}_N, P \in \boldsymbol{Z}_M, Q \in \boldsymbol{Z}_M\}$. The discrete states X and Y are used to reproduce nonlinear oscillatory behaviors of the basilar membrane, and the discrete states P and Q are used to control velocities of the discrete states X and Y, respectively. Then the following functions $g_x : \boldsymbol{Z}_N \times \boldsymbol{Z}_N \to \boldsymbol{R}$ and $g_y : \boldsymbol{Z}_N \times \boldsymbol{Z}_N \to \boldsymbol{R}$ are introduced.

$$\begin{aligned} g_x(X,Y) = {} & \delta l(X - N/2) - \omega l(Y - N/2) - \\ & l^3(X - N/2)((X - N/2)^2 - (Y - N/2)^2), \\ g_y(X,Y) = {} & \omega l(X - N/2) - \delta l(Y - N/2) - \\ & l^3(Y - N/2)((X - N/2)^2 - (Y - N/2)^2), \end{aligned}$$

where $l = m/N$, and $\delta \in \boldsymbol{R}$, $\omega \in \boldsymbol{R}$, and $m \in \boldsymbol{R}$ are parameters. Note that the functions g_x and g_y are used to design a vector field and are not implemented in hardware. Letting $\boldsymbol{Z}_M^{\pm} = \{-(M-1), \cdots, 0, \cdots, M-1\}$, the following discrete functions $F_X : \boldsymbol{Z}_N \times \boldsymbol{Z}_N \to \boldsymbol{Z}_M^{\pm}$ and $F_X : \boldsymbol{Z}_N \times \boldsymbol{Z}_N \to \boldsymbol{Z}_M^{\pm}$ are introduced.

$$f_X(X,Y) =$$

$$\begin{cases} M-1 & \text{if } \mathrm{Int}(\frac{l}{g_x(X,Y)T_X}) \geq M-1, \\ -(M-1) & \text{if } \mathrm{Int}(\frac{l}{g_x(X,Y)T_X}) \geq -(M-1), \\ \mathrm{Int}(\frac{l}{g_x(X,Y)T_X}) & \text{otherwise,} \end{cases}$$

$$f_Y(X,Y) =$$

$$\begin{cases} M-1 & \text{if } \mathrm{Int}(\frac{l}{g_y(X,Y)T_Y}) \geq M-1, \\ -(M-1) & \text{if } \mathrm{Int}(\frac{l}{g_y(X,Y)T_Y}) \geq -(M-1), \\ \mathrm{Int}(\frac{l}{g_y(X,Y)T_Y}) & \text{otherwise,} \end{cases}$$

where $T_X \in \boldsymbol{R}^+$ and $T_Y \in \boldsymbol{R}^+$ are periods of the following internal clocks C_X(t) and C_Y(t), respectively.

$$C_X(t) = \begin{cases} 1 & \text{if } t = 0, T_X, 2T_X, \cdots, \\ 0 & \text{if otherwise,} \end{cases}$$

$$C_Y(t) = \begin{cases} 1 & \text{if } t = 0, T_Y, 2T_Y, \cdots, \\ 0 & \text{if otherwise.} \end{cases}$$

Note that the ratio T_X/T_Y of the periods can be either rational (i.e., the clocks C_X and C_Y are phase-locked or synchronized) or irrational (i.e., the internal clocks C_X and C_Y are asynchronous). Since the clock generators are uncoupled, the period ratio T_X/T_Y is generically irrational and thus the internal clocks C_X(t) and C_Y(t) are generically asynchronous. Recall that the asynchronicity of the internal clocks C_X(t) and C_Y(t) are used to realize a smooth vector field of our model. The internal clocks C_X and C_Y trigger the following transitions of the discrete states P and Q, respectively.

If $C_X(t) = 1$, then

$$P(t_+) := \begin{cases} P(t)+1 & \text{if } P(t) < |F_X|, \\ 0 & \text{if } P(t) \geq |F_X|. \end{cases}$$

If $C_X(t) = 1$, then

$$Q(t_+) := \begin{cases} Q(t)+1 & \text{if } Q(t) < |F_Y|, \\ 0 & \text{if } Q(t) \geq |F_Y|. \end{cases}$$

Here the symbol "t_+" denotes "$\lim_{\epsilon \to +0} t + \epsilon$" and the symbol ":=" denotes an "instantaneous state transition" hereafter. The internal clocks C_X and C_Y trigger the following transitions of the discrete states X and Y, respectively.

If $C_X(t) = 1$ and $P(t) \geq |F_X|$, then

$$X(t_+) := \begin{cases} X(t)+1 & \text{if } X(t) \neq N-1 \\ & \text{and } F_X \geq 0, \\ X(t)-1 & \text{if } X(t) \geq 0 \\ & \text{and } F_X < 0, \\ X(t) & \text{otherwise.} \end{cases}$$

If $C_X(t) = 1$ and $Q(t) \geq |F_Y|$, then

$$Y(t_+) := \begin{cases} Y(t)+1 & \text{if } Y(t) \neq N-1 \\ & \text{and } F_Y \geq 0, \\ Y(t)-1 & \text{if } Y(t) \geq 0 \\ & \text{and } F_Y < 0, \\ Y(t) & \text{otherwise.} \end{cases}$$

Let

$$s(t) = A \sin(2\pi f t)$$

be a stimulation signal. Then the following stimulation input $S(t)$ is introduced.

$$S(t) = \begin{cases} 1 & \text{if } t = \tau_p(1), \tau_p(2), \cdots, \\ -1 & \text{if } t = \tau_n(1), \tau_n(2), \cdots, \\ 0 & \text{otherwise,} \end{cases} \tag{1}$$

where the instantaneous density of the pulse positions $\{\tau_p(1), \tau_p(2), \cdots, \}$ is proportional to $s(t)$ for $s(t) > 0$ and is zero for $s(t) \leq 0$; and the instantaneous density of the pulse positions $\{\tau_n(1), \tau_n(2), \cdots, \}$ is proportional to $-s(t)$ for $s(t) < 0$ and is zero for $s(t) \geq 0$. Note that such a density modulation can be easily realized by using a standard density modulator. The stimulation input $S(t)$ triggers the following transitions of the discrete state P and Q.

If $S(t) = 1$ and $F_X \geq 0$, then

$$P(t_+) := \begin{cases} P(t)+1 & \text{if } P(t) < |F_X|, \\ 0 & \text{if } P(t) \geq |F_X|. \end{cases}$$

If $S(t) = -1$ and $F_X \geq 0$, then

$$P(t_+) := \begin{cases} P(t)-1 & \text{if } P(t) > 0, \\ |F_X| & \text{if } P(t) = 0, \end{cases}$$

If $S(t) = 1$ and $F_X < 0$, then

$$P(t_+) := \begin{cases} P(t)-1 & \text{if } P(t) > 0, \\ |F_X| & \text{if } P(t) = 0, \end{cases}$$

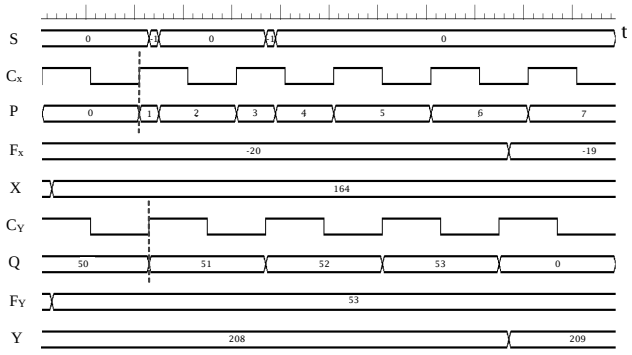

Figure 2: Typical time chart.

If $S(t) = -1$ and $F_X < 0$, then

$$P(t_+) := \begin{cases} P(t) + 1 & \text{if } P(t) < |F_X|, \\ 0 & \text{if } P(t) \geq |F_X|. \end{cases}$$

Then, the stimulation input $S(t)$ triggers the following transitions of the discrete state X and Y.

If $S(t) = 1$ and $F_X \geq 0$, then

$$X(t_+) := \begin{cases} X(t) + 1 & \text{if } X(t) \neq N - 1 \\ & \text{and } P(t) \geq |F_X|, \\ X(t) & \text{otherwise,} \end{cases}$$

If $S(t) = -1$ and $F_X \geq 0$, then

$$X(t_+) := \begin{cases} X(t) - 1 & \text{if } X(t) \neq 0 \\ & \text{and } P(t) = 0, \\ X(t) & \text{otherwise,} \end{cases}$$

If $S(t) = 1$ and $F_X < 0$, then

$$X(t_+) := \begin{cases} X(t) - 1 & \text{if } X(t) \neq 0 \\ & \text{and } P(t) = 0, \\ X(t) & \text{otherwise,} \end{cases}$$

If $S(t) = -1$ and $F_X < 0$, then

$$X(t_+) := \begin{cases} X(t) + 1 & \text{if } X(t) \neq N - 1 \\ & \text{and } P(t) \geq |F_X|, \\ X(t) & \text{otherwise.} \end{cases}$$

Fig. 2 shows a typical time chart of the model and Fig. 3 shows typical time waveforms of the model. In order to characterize the time waveforms, the following RMS of the discrete state X is introduced.

$$RMS(X) = \lim_{T \to \infty} \sqrt{\frac{l^2}{T} \int_T^{T_s} (X(t) - N/2)^2 dt}.$$

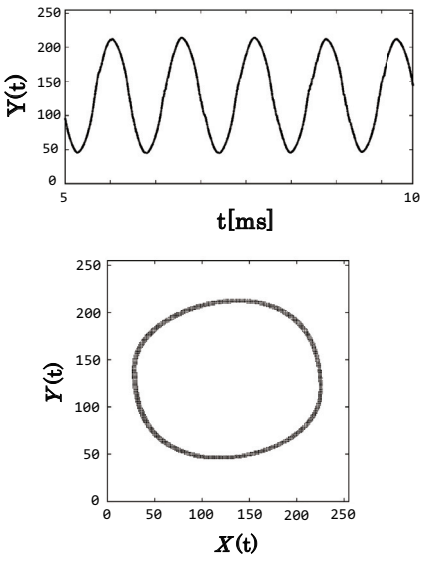

Figure 3: Typical time waveforms. The parameter values are (N, M, T_X, T_Y, δ, ω, m) = (256, 256, 10^{-7}, 10.1^{-7}, -10, $2\pi \times 10^3$, 64). The stimulation frequency is f = 1k[Hz].

In the case of Fig. 3, the RMS is about 67. Also, in order to characterize the stimulation input $S(t)$, the following magnitude p of $S(t)$ is introduced.

$$p(S) = \lim_{\tau \to \infty} \frac{\text{Number of spikes } |S(t)| = 1 \text{ for } t \in [0, \tau]}{\tau}$$

Using the magnitude p, the following sound power level SPL of $S(t)$ is introduced.

$$SPL(S) = (p(S) - p_0) \times 10^{-5}(\text{dB}),$$

where $p_0 = 1.0 \times 10^6$ is a reference magnitude corresponding to 0 (dB) of the SPL. Note that the sound power level SPL in this paper corresponds to a sound pressure level often used in the literatures on the physiology of cochlear. Using the SPL of the stimulation input $S(t)$ and the RMS of the discrete state X, the following minimum sound power level SPL_{min} is introduced.

Minimum sound power level SPL_{min}

The minimum sound power level SPL_{min} is the minimum sound power level SPL of the stimulation input S(t) such that the RMS of the discrete state X is greater than or equal to a given threshold value RMS_{th}.

Then, using the minimum sound power level SPL_{min} and the stimulation frequency f, the following frequency tuning curve is introduced.

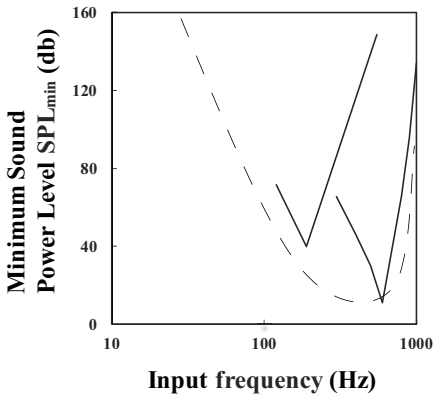

Figure 4: Frequency tuning curves of our model, where parameter values are the same as those in Fig. 3. The dashed line shows audible range which have 30-700[Hz] of a turtle [13]. It can be seen that the curves mimic some of the physiologically measured frequency tuning curves of the turtle in Fig. 1.

Frequency tuning curve

The characteristics curve of the minimum sound power level SPL_{min} with respect to the input frequency f is said to be a frequency tuning curve.

Fig. 4 shows frequency tuning curves of our model, where a dashed line shows audible range 30-700[Hz] of a turtle [13]. Comparing the frequency tuning curves in Fig. 4 (our model) and that in Fig. 1 (turtle), it can be seen that our model can mimic the physiologically measured frequency tuning curves of the turtle.

3. Conclusions

The nonlinear dynamics of a Hopf-bifurcation-type cochlea model based on a concept of an asynchronous bifurcation processor was investigated. It was shown that the model can reproduce nonlinear tuning curves of not only a mammalian cochlea (cat) but also a reptilian cochlea (turtle). Future problems are including (a) analysis of the occurrence mechanism of the bifurcation by using discrete-continuous hybrid Poincare map, (b) comparison of a frequency tuning curve of an FPGA-implemented circuit of our model with biological data, (c) reproductions of more highly nonlinear responses to sound stimuli such as multi-tone suppression, first and second pitch shifts, adaptation, parallel spike density encoding, and so on. This work was partially supported by JSPS KAKENHI Grant Number 15K00352.

References

[1] J. O. Pickes, An introduction to the physiology of hearing, 4th ed., Emerald Group Publishing 2012.

[2] M. P. Leong and C. T. Jin and P. H. W. Leong, An FPGA-Based Electronic Cochlea, EURASIP Journal on Applied Signal Processing, vol.7, 629-638, 2003.

[3] K. K. Charaziak and J. H. Siegel, Estimating Cochlear Frequency Selectivity with Stimulus-frequency Otoacoustic Emissions in Chinchillas, Journal of the Association for Research in Otolaryngology, 15, pp. 883-896, 2014.

[4] L. Watts, D. A. Kerns and R. F. Lyon, Improved Implementation of the Silicon Cochlea, IEEE Journal of Solid-State Circuits, vol. 27, pp. 692-700, 1992.

[5] R. V. Dundur, M. V. Latte, S.Y. Kulkarni, and M. K. Venkatesha, Digital Filter for Cochlear Implant Implemented on a Field- Programmable Gate Array, World Academy of Science, Engineering and Technology, 19, pp. 456-460, 2008.

[6] A. J. Hudspeth, F. Jiilicher and P. Martin, A critique of the critical cochlea: Hopf-a Bifurcation-Is better than none, J. Neurophysiol, vol. 104, pp. 1219-1229, 2010.

[7] M. Ospeck, Evidence of a Hopf bifurcation in frog hair cells, Biophysical Journal, vol. 80, pp. 2597-2607, 2001.

[8] M. Reit and W. Mathis and R. Stoop, Time-Discrete Nonlinear Cochlea Model Implemented on DSP for Auditory Studies, Nonlinear Dynamics of Electronic Systems, Proc. NDES 2012, pp. 1-4, 2012.

[9] F. Gomez, T. Lorimer, and R. Stoop, Signal-coupled subthreshold Hopf-type systems show a sharpened collective response, Physical Review Letters, 116, 108101, 2016.

[10] M. Izawa and H. Torikai, A Novel Hardware-Efficient Cochlea Model based on Asynchronous Cellular Automaton, Proc. IJCNN, paper ID 15745, 2015.

[11] K. Isobe and H. Torikai, A novel hardware-efficient asynchronous cellular automaton model of spike-timing dependent synaptic plasticity, IEEE Trans. CAS-II, 2016 (accepted).

[12] T. Noguchi and H. Torikai, Ghost Stochastic Resonance From an Asynchronous Cellular Automaton Neuron Model, IEEE Trans. CAS-II, vol. 60, pp. 111-115, 2013.

[13] A. C. Crawford and R. Fettipplace, The Frequency Selectivity of Auditory Nerve Fibres and Hair Cells In The Cochlea of The Turtle, J. Physiol, vol. 306, pp. 79-125, 1980.

[14] Y. Kuznetsov, Elements of Applied Bifurcation Theory, Springer, 2004.